# Polyvinyl pyrrolidone-assisted hydrothermal synthesis of octahedral $ZnFe_2O_4$ nanoparticles

*Zhanwen Pang[1], Mingliang Fang[1], Mingzai Wu[1,2], Yanmei Liu[1], Yongqing Ma[1], Xiansong Liu[1], Lide Zhang[2]*

[1]*Anhui Key Laboratory of Information Materials and Devices, Anhui University, Hefei 230039, People's Republic of China*
[2]*Key Laboratory of Materials Physics, Institute of Solid State Physics, Chinese Academy of Sciences, Hefei 230031, Anhui, People's Republic of China*
*E-mail: mz_wu@ustc.edu*

Published in Micro & Nano Letters; Received on 19th October 2011; Revised on 20th November 2011

Octahedral $ZnFe_2O_4$ nanocrystals were prepared via a polyvinyl pyrrolidone (PVP)-assisted hydrothermal route. X-ray diffractometer, field emission scanning electron microscopy and high-resolution transmission electron microscopy measurements were carried out to investigate the products' structures and morphologies. Different dosages of PVP were tested and 0.3 g was found to be the optimal dosage for the synthesis of octahedral $ZnFe_2O_4$. The selective adsorption of PVP onto the crystallographic planes should be responsible for the formation of the final octahedral particles. Moreover, magnetisation measurements revealed that these $ZnFe_2O_4$ particles possessed a high magnetic parameter with a saturation magnetisation of 44.30 emu/g and a coercivity of 299.2 Oe at room temperature.

**1. Introduction:** Zinc ferrite, an important member of spinel structure ferrite family, has aroused much interest owing to its potential applications in drug carriers, magnetic recording, gas sensor, semiconductor devices and catalysis [1–5]. In recent years, many methods have been reported for the synthesis of various interesting $ZnFe_2O_4$ nanostructures, including nanofibres [1], nanotube [2], nanoplates [3], quasi-cube [4] and hollow spherical ones [5]. For example, fibre-like $ZnFe_2O_4$ nanocrystals were obtained by thermal treatment of the precursors [1]. Plate-like $ZnFe_2O_4$ particles were successfully synthesised in liquid polyols at elevated temperature [3]. Quasi-cube $ZnFe_2O_4$ nanocrystals were reported by the reduction of ferric chloride hexahydrate and zinc chloride in the presence of sodium dodecyl sulphate [4]. Although much achievement has been made in the morphological control of $ZnFe_2O_4$ nanoparticles, there are few reports on the synthesis of crystalline octahedral $ZnFe_2O_4$ via a hydrothermal route except the ammonia solution method using metal Zn sheet and $FeCl_2$ as starting materials [6].

Recently, the synthesis of octahedrons composed of eight {1 1 1} crystal planes have been the focus of intensive research [7–9]. For example, Au nano-octahedrons with well-defined shape have been reported because of its attractive optical properties [7]. Magnetite micro-octahedrons prepared via a biomolecule-assisted hydrothermal route was reported to exhibit a discharge capacity of ca. 600 mA $g^{-1}$ in the first cycle and a discharge voltage of 0.92 and 0.74 V, respectively [8]. Most recently, $Mn_3O_4$ micro-octahedrons exhibited an enhanced specific capacitance of 322 F $g^{-1}$ compared with the truncated octahedrons with specific capacitances of 244 F $g^{-1}$ [9]. As is well known, the properties of nanomaterials are strongly dependent on the morphology of their internal structures [10, 11], such as the octahedral $ZnFe_2O_4$ nanoparticles are expected to show some novel physical, chemical properties.

Hydrothermal processing enables the synthesis of many crystalline materials without a calcination step at the temperatures of 200°C and lower and can yield some metastable products on a large scale, which has attracted much attention around the world. In this Letter, we present a scalable synthesis of octahedral $ZnFe_2O_4$ nanoparticles using zinc nitrate hexahydrate and ferric nitrate nonahydrate as staring materials via a simple hydrothermal procedure, which minimise the problem of instability of $Fe^{2+}$ ions and the higher cost. Moreover, the octahedral $ZnFe_2O_4$ nanaocrystals possess a higher coercivity (about 299.2 Oe), which make these octahedral $ZnFe_2O_4$ nanaocrystals have a widespread potential application in tumour therapy, semiconductor devices, magnetic recording and drug carriers.

**2. Experimental:** For the present experiment, all the reagents are of analytical grade and used as received. In a typical synthesis, zinc nitrate hexahydrate [0.5 mmol], ferric nitrate nonahydrate [1.0 mmol], polyvinyl pyrrolidone (PVP) [0.3 g] and urea [4.5 mmol] were dissolved in 20 ml distilled water. After being vigorously stirred for 30 min, 3 ml of ammonia and 3 ml of hydrazine were added dropwise into the above mixture solution, respectively. Subsequently, 9 mmol of sodium hydroxide was added to raise the solution pH to 13. Finally, the solution was transferred into a Teflon-lined stainless steel autoclave with 40 ml capacity, which was sealed and maintained at 180°C for 8 h before being left to cool to room temperature naturally. The resulting black solid powder was collected by centrifugation and washed with alcohol and distilled water three times, respectively. Then the sample was dried at 50°C for 5 h. The as-obtained sample was labelled as $S_{0.3}$, with 0.3 indicating the dosage of PVP 0.3 g. The same reactions were performed for the case of 0, 0.1 and 0.6 g PVP with other reaction parameters kept unchanged, yielding samples $S_0$, $S_{0.1}$ and $S_{0.6}$, respectively.

The structures, morphologies and microstructures of these three samples were characterised by X-ray powder diffraction (XRD) using an 18 kW advanced X-ray diffractometer with Cu K$\alpha$ radiation ($\lambda = 1.54056$ Å), scanning electron microscopy (SEM) and transmission electron microscopy (TEM). Magnetic hysteresis loops were measured on a vibrating sample magnetometer (VSM, BHV-55) at room temperature.

**3. Results and discussions:** Fig. 1 shows the XRD patterns of samples $S_0$, $S_{0.3}$ and $S_{0.6}$. All of the diffraction peaks for these three samples can be indexed to the spinel $ZnFe_2O_4$ (JCPDS No. 22-1012). No other peaks of impurities are observed. After careful check, we can find that a weak peak (1 1 1) only occurred in sample $S_{0.3}$. The crystallite size can be calculated from X-ray line broadening using the Scherrer equation: $D = 0.89\lambda/\beta\cos\theta$, where $D$ is the average crystal size in nm, $\lambda$ is the Cu K$\alpha$ wavelength (0.15406 nm), $\beta$ is the full-width at half-maximum (FMWH) and $\theta$ is the diffraction angle. Compared with samples $S_0$ and $S_{0.6}$, the obvious reduction of FMWH of peak (3 1 1) for sample $S_{0.3}$ indicates that $S_{0.3}$ possesses a biggest crystalline size (estimated to be 95 nm). Both the occurrence of weak peak (1 1 1) and the obvious reduction of FMWH of peak (3 1 1) in




doi: 10.1049/mnl.2011.0565

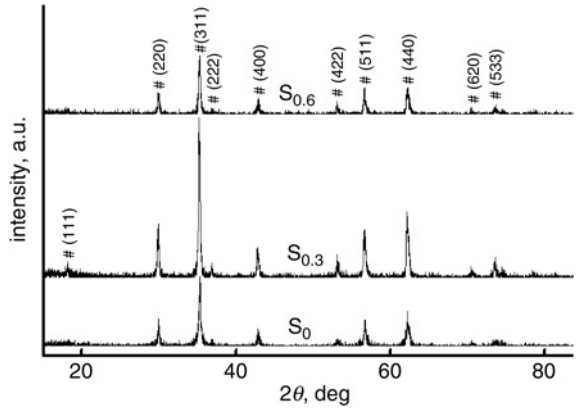


**Figure 1** *XRD patterns of the samples $S_0$, $S_{0.3}$ and $S_{0.6}$*

sample $S_{0.3}$ suggest that the dosage of 0.3 g PVP is favourable to the crystalline growth. Moreover, the ratio of reflection intensity of peak (3 1 1) to that of peak (1 1 1) for sample $S_{0.3}$ is much stronger than that for bulk materials in the JCPDS card, indicating the presence of possible orientation for sample $S_{0.3}$. The lattice parameter is calculated to be 0.84438 nm based on the (3 1 1) reflection, very close to that of the bulk $ZnFe_2O_4$ (0.84411 nm).

The morphology and microstructure of sample $S_{0.3}$ was characterised by SEM and high-resolution TEM (HRTEM), as shown in Fig. 2. A panoramic SEM image shows that octahedron-like nanostructures dominates the as-prepared $ZnFe_2O_4$ nanocrystals with size distributed between 90 and 110 nm and the facets of these octahedrons are apparently distinguishable (Fig. 2*a*). HRTEM study was further conducted to investigate the detailed morphology. After careful check, many octahedral particles could be found in Fig. 2*b*. Fig. 2*c* shows the lattice fringe and selected area electron diffraction (SAED) of the boxed area in Fig. 2*b*. The perfect lattice fringes and distinct diffraction spots reveals the single crystal feature of the octahedral $ZnFe_2O_4$. On the basis of the HRTEM image, the planar distance of lattice fringes is evaluated to be 0.48 nm, consistent with the (1 1 1) interplanar spacing of spinel $ZnFe_2O_4$. Considering the structure symmetry, combined with the results of XRD, SEM, HRTEM analysis, it can be concluded that the $ZnFe_2O_4$ octahedron is bounded by eight {1 1 1} planes. A structure model of the octahedral $ZnFe_2O_4$ is presented in Fig. 2*d*.

Different dosages of PVP were used to modulate the reaction and to control the morphologies. In the absence of PVP, few quasi-octahedral particles are formed, as shown in Fig. 3*a*. When the surfactant dosage is increased to 0.1 g, a small quantity of octahedron-like particles are produced (Fig. 3*b*). With the increase of surfactant dosage to 0.3 g, a large number of octahedron-like particles with facets apparently distinguishable coexists with minute quantity of small powders, as shown in Fig. 3*c*. When the surfactant dosage is increased to 0.6 g, the number of octahedron-like particles is reduced significantly, as shown in Fig. 3*d*. In fact, the PVP dosages of 0.4 and 0.5 g were also investigated and the obtained products were found to have similar morphologies to that of the case of 0.6 g PVP, which was not shown here. All of these results indicate that the surfactants have significant effects on the stages of crystal growth, and the optimal dosage for the synthesis of octahedral particles is 0.3 g, which is consistent with the XRD analysis. Furthermore, no agglomeration of particles could be found in the SEM images.

For our case, the morphology evolution can be explained in terms of Ostwald ripening [12] and the crystal surface energy changes when appropriate amount of PVP is adsorbed onto specific facets of the $ZnFe_2O_4$ crystal, similar to the growth mechanism of the Ag crystal [13]. First, lots of small $ZnFe_2O_4$ particles are formed, governed by the cationic/anionic mixture reaction system.

$$Zn^{2+} + 2Fe^{3+} + 8OH^- \rightarrow ZnFe_2O_4 + 4H_2O$$

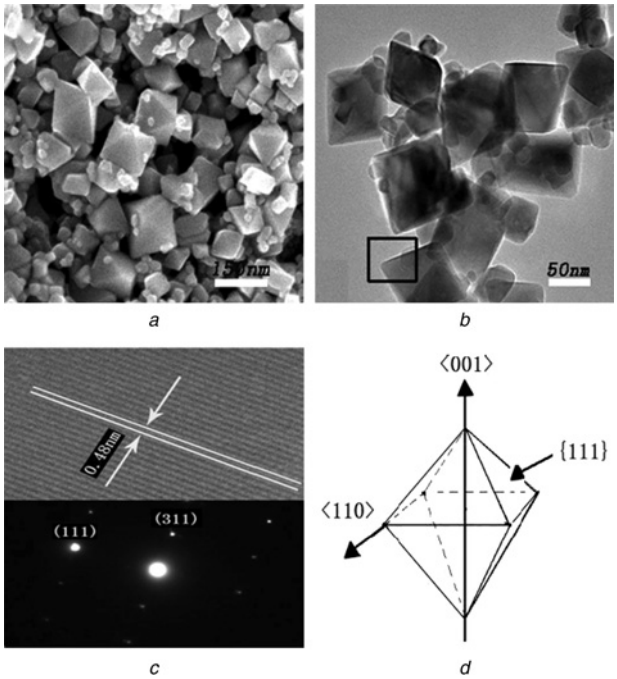


**Figure 2** *SEM, HRTEM images of sample $S_{0.3}$*
*a* Lower magnification SEM image of sample $S_{0.3}$
*b* TEM image of sample $S_{0.3}$
*c* Lattice fringe and SAED of the part labelled with rectangle pane in Fig. 2*b*
*d* Computer-aided design models of single sample

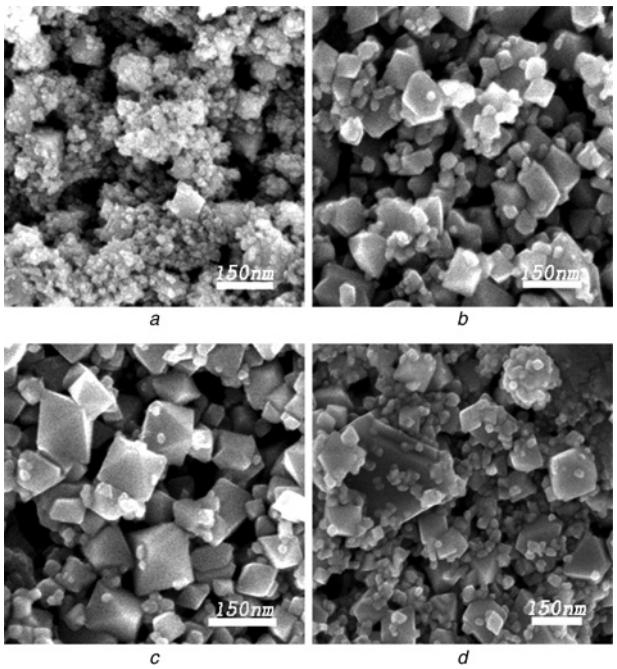


**Figure 3** *SEM images of samples*
*a* Sample $S_0$
*b* Sample $S_{0.1}$ obtained at 180°C for 8 h, with 0.1 g PVP
*c* Sample $S_{0.3}$
*d* Sample $S_{0.6}$

These preformed $ZnFe_2O_4$ particles serve as seeds, on which $Zn^{2+}$ and $Fe^{3+}$ further deposit and grow. For spinel $ZnFe_2O_4$ with cubic crystal structure, all the atoms inside are bonded to six neighbours and are quite stable, but atoms on the surface are only bonded to five neighbours or less, which makes these surface atoms less stable. Larger particles are more energetically favourable. As the system tries to lower its overall energy, $Zn^{2+}$ and $Fe^{3+}$ on the surface of a small particle with only 4 or 5 bonded neighbours will tend to detach from the particle, and diffuse into the solution, which will finally recrystallise onto the surface of larger particles. This is the Ostwald ripening process. Therefore smaller particles with size smaller than a critical value will shrink, while larger particles further grow. This could explain the coexistence of smaller particles with the larger octahedral particles. Moreover, owing to the selective adsorption [12, 13] of PVP and the difference of free energies of the crystallographic plane ($\gamma\{1\ 1\ 0\} > \gamma\{1\ 0\ 0\} > \gamma\{1\ 1\ 1\}$) [14, 15], PVP molecule would be preferentially absorbed onto the {1 1 1} surface with lower surface energy [13–15]. Thus, the growth rate of <1 0 0> and <1 1 0> orientation is faster than that of <111> orientation, resulting in the disappearance of {1 0 0} and {1 1 0} surface during growth. Finally, the seeds become octahedral nanocrystalline bounded by eight {1 1 1} planes. Moreover, the more dosage of PVP does not mean the better shape control, which could be explained based on the fact that the equilibrium constant for PVP molecules binding to crystal faces of $ZnFe_2O_4$ would change with the increase of PVP dosage, resulting in the changes of the growth rate and the morphologies of the final products.

The static magnetic property of the samples $S_0$, $S_{0.3}$ and $S_{0.6}$ are measured at room temperature, as shown in Fig. 4. The inset is the magnetised hysteretic loops at low applied field. Compared with $S_0$ and $S_{0.6}$, sample $S_{0.3}$ exhibited a higher saturated magnetisation, further supporting the fact that the dosage of 0.3 g PVP is favourable to the crystalline crystallise. The smooth particles' surfaces shown in Fig. 2 and the XRD intensity in Fig. 1 confirm the above analysis. The value of the saturated magnetisation ($M_s$), remnant magnetisation ($M_r$) and coercivity ($H_c$) are 44.30 emu/g, 17.37 emu/g and 299.2 Oe, respectively, all of which are higher than those (0.33 emu/g, 27 Oe) reported for $ZnFe_2O_4$ powders in [16].

Bulk zinc ferrite is a completely normal spinel structure with $Zn^{2+}$ ions located in A sites and $Fe^{3+}$ ions in B sites. Thus, there is no superexchange interaction between A and B sites. In our system, tetrahedral A sites are occupied with some $Fe^{3+}$ ions and switch on the $Fe^{3+}$(A)–O2–$Fe^{3+}$(B) superexchange interaction and should be responsible for the high magnetic parameter. In fact, when the size of the particles is reduced to nano-scale, the surface/volume ratio of the particles can be increased notably, so that up to 50% of the particle atoms can be located on the surface and directly influence the magnetic properties of the particles [17]. For the sample $S_{0.3}$, a large fraction of the total spins at the surface will have a non-collinear configuration different from that of the core ones, due to broken exchange bonds and symmetry of the octahedral. The higher magnetic parameters of these octahedron-like $ZnFe_2O_4$ particles should have a widespread potential application in magnetic recording, drug carriers and catalysis.

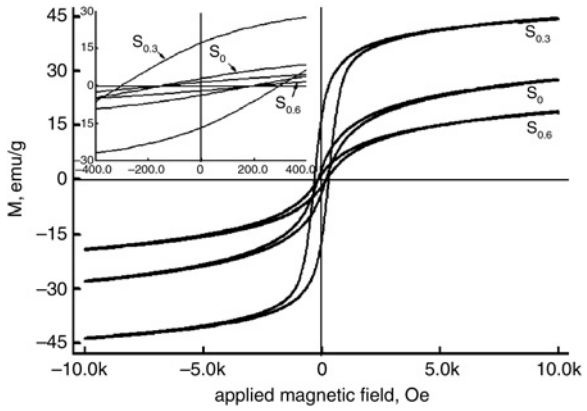


**Figure 4** *Magnetisation curve for the samples $S_0$, $S_{0.3}$ and $S_{0.6}$ measured at room temperature*

**4. Conclusion:** Octahedral $ZnFe_2O_4$ nanoparticles with a crystalline size of about 95 nm were successfully synthesised by a simple hydrothermal reaction. The dosage of PVP played an important role in the morphological control of the products. 0.3 g was found to be enough for the complete disappearance of {1 0 0} and {1 1 0} planes and should be the optimal dosage for the octahedral $ZnFe_2O_4$ synthesis. Magnetisation measurement shows that octahedral $ZnFe_2O_4$ has a high magnetic parameter, whose saturated magnetisation ($M_s$) and coercivity ($H_c$) are 44.30 emu/g and 299.2 Oe, respectively.

**5. Acknowledgment:** This work was financed by the 211 project of Anhui University, National Natural Science Foundation of China (50901074, 50672001), Anhui Provincial Natural Science Fund (11040606M49) and Innovation Project of Anhui University Graduate Education (yqh090010).

## 6 References

[1] Li Q.L., Bo C.C., Wang W.T.: 'Preparation and magnetic properties of $ZnFe_2O_4$ nanofibers by coprecipitation-air oxidation method', *Mater. Chem. Phys.*, 2010, **124**, pp. 891–893

[2] Liu F.F., Li X.Y., Zhao Q.D., Hou Y., Quan X., Chen G.H.: 'Structural and photovoltaic properties of highly ordered $ZnFe_2O_4$ nanotube arrays fabricated by a facile sol-gel template method', *Acta Mater.*, 2009, **57**, pp. 2684–2690

[3] Cao X.B., Gu L., Lan X.M., Zhao Z., Yao D., Sheng W.J.: 'Spinel $ZnFe_2O_4$ nanoplates embedded with Ag clusters: preparation, characterization, and photocatalytic application', *Mater. Chem. Phys.*, 2007, **106**, pp. 175–180

[4] Zhang G.Y., Sun Y.Q., Gao D.Z., Xu Y.Y.: 'Quasi-cube $ZnFe_2O_4$ nanocrystals: hydrothermal synthesis and photocatalytic activity with $TiO_2$ (Degussa P25) as nanocomposite', *Mater. Res. Bull.*, 2010, **45**, pp. 755–760

[5] Guo X.W., Lu X., Fang X.P., *ET AL.*: 'Lithium storage in hollow spherical $ZnFe_2O_4$ as anode materials for lithium ion batteries', *Electrochem. Commun.*, 2010, **12**, pp. 847–850

[6] Yu S.H., Fujino T., Yoshimura M.: 'Hydrothermal synthesis of $ZnFe_2O_4$ ultrafine particles with high magnetization', *J. Magn. Magn. Mater.*, 2003, **256**, pp. 420–424

[7] Li C.C., Shuford K.L., Park Q.H., *ET AL.*: 'High-yield synthesis of single-crystalline gold nano-octahedra', *Angew. Chem. Int. Ed.*, 2007, **46**, pp. 3264–3268

[8] Qu X.F., Zhou G.T., Yao Q.Z., Fu S.Q.: 'Aspartic-acid-assisted hydrothermal growth and properties of magnetite octahedrons', *J. Phys. Chem. C*, 2010, **114**, pp. 284–289

[9] Jiang H., Zhao T., Yan C.Y., Ma J., Li C.Z.: 'Hydrothermal synthesis of novel $Mn_3O_4$ nano-octahedrons with enhanced supercapacitors performances', *Nanoscale*, 2010, **2**, pp. 2195–2198

[10] Wu M.Z., Xiong Y., Jia Y.S., *ET AL.*: 'Magnetic field-assisted hydrothermal growth of chain-like nanostructure of magnetite', *Chem. Phys. Lett.*, 2005, **401**, pp. 374–379

[11] Wang J., Chen Q.W., Zeng C., Hou B.Y.: 'Magnetic-field-induced growth of single-crystalline $Fe_3O_4$ nanowires', *Adv. Mater.*, 2004, **16**, pp. 137–140




doi: 10.1049/mnl.2011.0565

[12] Lorenz R., Voorhees P.W.: 'Growth and coarsening: Ostwald ripening in material processing' (Springer, 2002), pp. 117–118
[13] Tao A.R., Sinsermsuksakul P., Yang P.D.: 'Polyhedral silver nanocrystals with distinct scattering signatures', *Angew. Chem. Int. Ed.*, 2006, **45**, pp. 4597–4601
[14] Sun Y.G., Xia Y.N.: 'Shape-controlled synthesis of gold and silver nanoparticles', *Science*, 2002, **298**, pp. 2176–2179
[15] Wang Z.L.: 'Electron microscopy of shape-controlled nanocrystals and their assemblies', *J. Phys. Chem.*, 2000, **104**, pp. 1153–1175
[16] Mozaffari M., EghbaliArani M., Amighian J.: 'The effect of cation distribution on magnetization of $ZnFe_2O_4$ nanoparticles', *J. Magn. Magn. Mater.*, 2010, **322**, pp. 3240–3244
[17] Yao C.W., Zeng Q.S., Goya G.F., *ET AL.*: '$ZnFe_2O_4$ nanocrystals: synthesis and magnetic properties', *J. Phys. Chem. C*, 2007, **111**, pp. 12274–12278